NeuroImage **16,** 283–294 (2002)
doi:10.1006/nimg.2002.1110, available online at http://www.idealibrary.com on IDEAL®

Repeated fMRI Using Iron Oxide Contrast Agent in Awake, Behaving Macaques at 3 Tesla

Francisca P. Leite,* Doris Tsao,† Wim Vanduffel,†,§ Denis Fize,‡ Yuka Sasaki,§ Larry L. Wald,§ Anders M. Dale,§ Ken K. Kwong,§ Guy A. Orban,‡ Bruce R. Rosen,§ Roger B. H. Tootell,§ and Joseph B. Mandeville§

**Massachusetts Institute of Technology, Department of Nuclear Engineering, Cambridge, Massachusetts 02139; †Department of Neurobiology, Harvard Medical School, Cambridge, Massachusetts 02115; ‡Laboratorium voor Neuro-en Psychofysiologie, Katholieke Universiteit Leuven, Campus Gasthuisberg, Leuven B-3000, Belgium; and §Massachusetts General Hospital and Athinoula A. Martinos Center for Biomedical Imaging, Charlestown, Massachusetts 02129*

Received October 8, 2001

Iron oxide contrast agents have been employed extensively in anesthetized rodents to enhance fMRI sensitivity and to study the physiology of cerebral blood volume (CBV) in relation to blood oxygen level-dependent (BOLD) signal following neuronal activation. This study quantified the advantages of exogenous agent for repeated neuroimaging in awake, nonhuman primates using a clinical 3 Tesla scanner. A monocrystalline iron oxide nanoparticle (MION) solution was injected at iron doses of 8 to 10 mg/kg in two macaque monkeys. Adverse behavioral effects due to contrast agent were not observed in either monkey using cumulative doses in excess of 60 mg/kg. Relative to BOLD imaging at 3 Tesla, MION increased functional sensitivity by an average factor of 3 across the brain for a stimulus of long duration. Rapid stimulus presentation attenuated MION signal changes more than BOLD signal changes, due to the slower time constant of the blood volume response relative to BOLD signal. Overall, the contrast agent produced a dramatic improvement in functional brain imaging results in the awake, behaving primate at this field strength.

INTRODUCTION

The awake, behaving macaque is an important model of the human brain for neuroscience, physiology, and the development of neuroimaging methodologies. The use of alert animals expands the range of experimental paradigms, and such studies eliminate the significant complications and uncertain interpretation associated with anesthesia. Results obtained in awake nonhuman primates also require less extrapolation to studies of the alert human brain and to the extensive literature on the organization of macaque brain that has been derived from invasive methods. As a complimentary noninvasive imaging tool, fMRI serves as a powerful whole-brain survey technique that can be performed repeatedly in individual animals.

Functional MRI based on blood oxygen level-dependent (BOLD) signal has become a routine tool of human neuroscience, and several groups have previously reported fMRI results in anesthetized or awake nonhuman primates using BOLD contrast (Stefanacci *et al.,* 1998; Dubowitz *et al.,* 1998; Logothetis *et al.,* 1999; Hayashi *et al.,* 1999; Disbrow *et al.,* 2000; Logothetis *et al.,* 2001; Vanduffel *et al.,* 2001). However, the low sensitivity of the BOLD method at common magnetic field strengths presents a challenge for the detection of subtle changes in local perfusion, and sensitivity is one factor that limits high spatial resolution.

In animal models, exogenous MRI contrast agents with long blood half lives provide an attractive alternative to BOLD signal. In particular, dextran-coated iron oxide agents (Weissleder *et al.,* 1990; Josephson *et al.,* 1990) have found utility in a wide variety of animal research and are now being tested in human clinical trials (Sharma *et al.,* 1999; Taylor *et al.,* 1999; Enochs *et al.,* 1999). For functional brain mapping in anesthetized rodents, these agents have demonstrated significant advantages over BOLD signal in terms of functional sensitivity at 2 and 4.7 Tesla (Mandeville *et al.,* 1998; Kennan *et al.,* 1998; van Bruggen *et al.,* 1998; Chen *et al.,* 2001). Furthermore, such contrast agent studies are uniquely suited for spatial-temporal comparisons of the physiology of cerebral blood volume (CBV) in relation to BOLD signal, which depends upon blood volume, blood flow, and oxygen utilization. Rodent studies using electrical forepaw stimulation have shown that the temporal evolution of CBV differs markedly from BOLD signal (Mandeville *et al.,* 1998) and cerebral blood flow (Mandeville *et al.,* 1999b).

Due to the difficulties of obtaining robust BOLD responses in the presence of motion artifacts in awake

1053-8119/02 $35.00

primates, as described by others (Stefanacci *et al.*, 1998; Logothetis *et al.*, 1999), two recent studies have explored the viability of contrast agents for fMRI studies in alert primates. Dubowitz *et al.*, (2001) found that a low dose of an iron oxide agent enabled a modest improvement in functional sensitivity relative to BOLD signal at 1.5 Tesla. Vanduffel *et al.* (Vanduffel *et al.*, 2000; Mandeville *et al.*, 2001b; Vanduffel *et al.*, 2001) demonstrated that contrast agent enabled a robust mapping of motion-sensitive regions throughout visual cortex at this same field strength and that this method provided better sensitivity and apparent localization than BOLD signal.

We report results from a series of experiments in awake, behaving macaques using repeated injections of iron oxide contrast agent at doses that are effective for functional brain imaging. We characterized the temporal relationship of functional signals weighted by deoxyhemoglobin and blood volume using a variety of stimulus designs, and we compared the functional sensitivity of contrast-enhanced fMRI in relation to BOLD signal at 3 Tesla for short, prolonged, and rapidly presented stimuli. These results, and the macaques' apparent tolerance of repeated injections of iron oxide, show that this method is both viable and highly advantageous for functional brain imaging in awake primates.

METHODS

Animal Model

All experiments were performed at the Massachusetts General Hospital according to NIH and European animal care guidelines, following the general procedures as employed at a different laboratory (Vanduffel *et al.*, 2001). Briefly, plastic headsets were surgically implanted onto the skulls of two male rhesus monkeys (monkeys "M-A" and "M-B", 2.5–3 kg) during anesthesia. Operations were performed under isoflurane (1.5%)/N_2O (50%)/O_2 (50%). Antibiotics (50 mg/kg i.m., Kefzol, Lilly, Brussels) and analgesics (4 mg/kg i.m. Dolzam, Zambon, Brussels) were given daily for 3–7 days following each surgery.

After recovery, monkeys were adapted to physical head restraint while seated on their haunches in the "sphinx" position inside a plastic box. Animals were trained to perform a high acuity fixation task while visual stimuli were presented in the background. When a small vertical fixation bar (5 × 18-min arc) switched to a horizonal orientation, a monkey could obtain a reward of apple juice by quickly placing a hand to interrupt a light path. Incorrect responses were penalized by a delay before presentation of the next horizontal bar. All responses were recorded and monitored on-line to determine performance accuracy and the monkeys' willingness to continue. Despite the fact that the monkeys' response scores were consistently high, direct eye monitoring showed repeated saccades from the fixation point, so retinotopic activation patterns presumably contain some contamination from spurious eye movement.

For all studies that employed the monocrystalline iron oxide nanoparticle (MION) contrast agent, the MION solution was injected into the femoral vein below the knee just prior to each scanning session; no additional MION was added during the duration of a scan. MION was synthesized at the Massachusetts General Hospital (Weissleder *et al.*, 1990; Shen *et al.*, 1993) and is widely distributed throughout the MRI community. MION was injected in the original production buffer of sodium citrate without saline dilution. An iron dose of 8–10 mg/kg was injected in a volume of 1.8–2 ml using a MION solution with a concentration of 11.92 mg iron per milliliter.

Visual Stimulation

Visual stimuli were projected from an LCD projector (Sharp model XG-NV6XU) onto a screen which was positioned 29.5 cm in front of the monkey's eyes. The visual stimulus was a pinwheel checkerboard in which black and white segments were alternated at 8 Hz. This stimulus, with a mean luminance of 1795 cd/m^2, was compared to a baseline condition of a spatially uniform gray screen with a luminance of 12 cd/m^2. The stimulus covered a visual field of 37 × 48°, and the fixation bar (0.8 × 0.2°) was presented at the center of the visual field at all times.

Four stimulus paradigms, each lasting 4.5 min, were employed. Each paradigm included 30 s of baseline at the beginning of the run, and then used the following timing during the remaining four minutes: (1) 2 cycles of 60 s of stimulus followed by 60 s of baseline, (2) 4 cycles of 4 s of stimulus followed by 56 s of baseline, (3) 8 cycles of 4 s of stimulus followed by 26 s of baseline, and (4) 16 cycles of 4 s of stimulus followed by 8 s of baseline, with an additional 48 s of baseline at the end.

For the 60-s stimulus paradigm, we acquired 22 BOLD runs in 3 sessions and 11 MION runs in 2 sessions for monkey M-A. For monkey M-B, we acquired 34 BOLD runs in 7 sessions and 16 MION runs in 3 sessions. Runs with different stimulus paradigms were cycled during each session, so the numbers of runs were similar for the other paradigms. Scanning sessions typically lasted 3 h.

Magnetic Resonance Imaging

Experiments were performed in a 3 Tesla Siemens Allegra scanner (Siemens Medical System, Erlangen, Germany) using a custom surface coil for radio frequency excitation and reception of signal. All functional imaging employed single shot multislice echo planar imaging with an isotropic resolution of 1.5 mm.

20 slices were acquired using a repetition time of 2 s and a 90° flip angle for the visual paradigm that alternated 60 s of stimulus with 60 s of baseline. For all other visual paradigms, 4 slices through primary visual cortex were acquired using a repetition time of 500 ms and a flip angle of 45°. All BOLD studies employed a gradient echo time of 30 ms, and all MION studies used a gradient echo time of 20 ms (the minimum achievable value for the selected resolution and sequence).

In addition to functional imaging, T1-weighted EPI images were acquired in each session in order to facilitate registration of brains across magnet sessions by improving the anatomical detail relative to BOLD images. Additionally, data were acquired in each session to enable the calculation of T_2^* maps by obtaining 9 gradient echo times from 20 to 60 ms at 5-ms intervals. These data were collected at the beginning of each BOLD session and at both the beginning and end of each MION session.

Data Analysis

Despite physical fixation of the monkeys' heads in the restraint device, apparent brain motion and small distortions resulted from changes in the magnetic field associated with body motion. Therefore, motion correction was applied to all data sets using the Analysis of Functional NeuroImages (AFNI) motion correction algorithm (Cox and Hyde, 1997). For each animal, all images acquired in all sessions were then registered into a common space in order to enable spatio-temporal comparisons of BOLD and MION signals, and to enable comparison of T_2^* and R_2^* ($1/T_2^*$) maps between BOLD and MION sessions. In order to minimize imperfections in registration, all data were spatially smoothed after registration using an isotropic gaussian filter with a full-width at half-maximum of 3 mm.

R_2^* and T_2^* maps were computed from the multi-echo data assuming monoexponential relaxation of MRI signal: $S(T_E) = S(0)\exp(-T_E/T_2^*)$. The blood iron concentration was monitored through the transverse relaxation rate due to MION in the blood: $R_2^{*,\mathrm{MION}} = R_2^* - \overline{R_2^{*,\mathrm{BOLD}}}$, where R_2^* is the relaxation rate determined from the multiecho data and the BOLD relaxation rate refers to the average value of the total relaxation rate across BOLD sessions at each voxel. The iron blood half life ($T_{1/2}$) was then estimated from a monoexponential decay function across the duration of each experiment: $R_2^{*\mathrm{MION}}(t) = R_2^{*\mathrm{MION}}(0)\exp(-0.69\ t/T_{1/2})$.

When averaging MION signal changes across sessions, it is necessary in principle to account for the different blood concentrations of iron oxide. One way to properly account for inter-session effects of dose is to convert signal to percent CBV change, as done in rodent experiments when contrast agent is injected inside the magnet (e.g., Mandeville *et al.*, 1998). Because contrast agent was injected outside the magnet in these experiments for logistical reasons, we used a global normalization factor for each session to generate a corrected change in transverse relaxation rate:

$$\Delta R_2^{*\mathrm{CORR}}(t) = \{R_2^{*\mathrm{MION,AVERAGE}}/R_2^{*\mathrm{MION,SESSION}}\}\Delta R_2^{*\mathrm{SESSION}}(t),$$

where the relaxation rates were determined across a large brain volume during each session as described above, and the average relaxation rate is the average across sessions. Relative to voxel-wise calculations of percent changes in CBV, the global correction is less susceptible to intersession differences in the magnetic field shim and imperfections in cross-session alignment. Nevertheless, percentage CBV calculations can be expected to be accurate across relatively large regions of interest, as used for the generation of our time course figures.

Analysis of functional data employed general linear model methods (Friston *et al.*, 1995; Boynton *et al.*, 1996), in which a hemodynamic impulse response function (IRF) is convolved with the stimulus paradigm to generate a maximum likelihood estimation of the stimulus-linked vascular response. We determined separate BOLD and MION IRFs from a region of interest analysis applied to each of the respective data sets. To characterize the temporal response, a 1-cm^3 region of interest was selected from primary visual cortex using the registered data sets. In each case, the IRF for subsequent analysis was assembled from a series of exponential basis functions, $h(t) = \sum_k a_k/\tau_k\ exp(-t/\tau_k)$. In this basis, convolution with a step function generates a hemodynamic response $H(t) = \sum_k a_k\ (1 - exp(-t/\tau_k))$ following stimulus onset, and $H(t) = \sum_k a_k\ exp(-t/\tau_k)$ following stimulus cessation. Thus, this formulation provides flexibility and the advantage of simplicity, in that the dominant low frequency time constants can be measured directly from the data. The amplitudes of the basis functions for each IRF were fit within the general linear model after inclusion of a constant term and a linear drift. The data for all four stimulation paradigms were fit simultaneously in order to provide an optimal estimate of the IRF.

After describing the temporal response, the statistical power of the BOLD and MION methods were measured using standard linear model methods (Friston *et al.*, 1995) and the IRFs as determined from the region of interest analyses. Specifically, if N data points (**d**) as a function of time (t) are a simple linear summation of n basis functions (**B**) times parameters (**P**) within a given error (**e**), $\boldsymbol{d}_t = \sum_j \boldsymbol{B}_{tj}\boldsymbol{P}_j + e_t$, then the contrast-to-noise ratio (CNR) for a simple two-state comparison can be calculated as a T statistic: $T =$

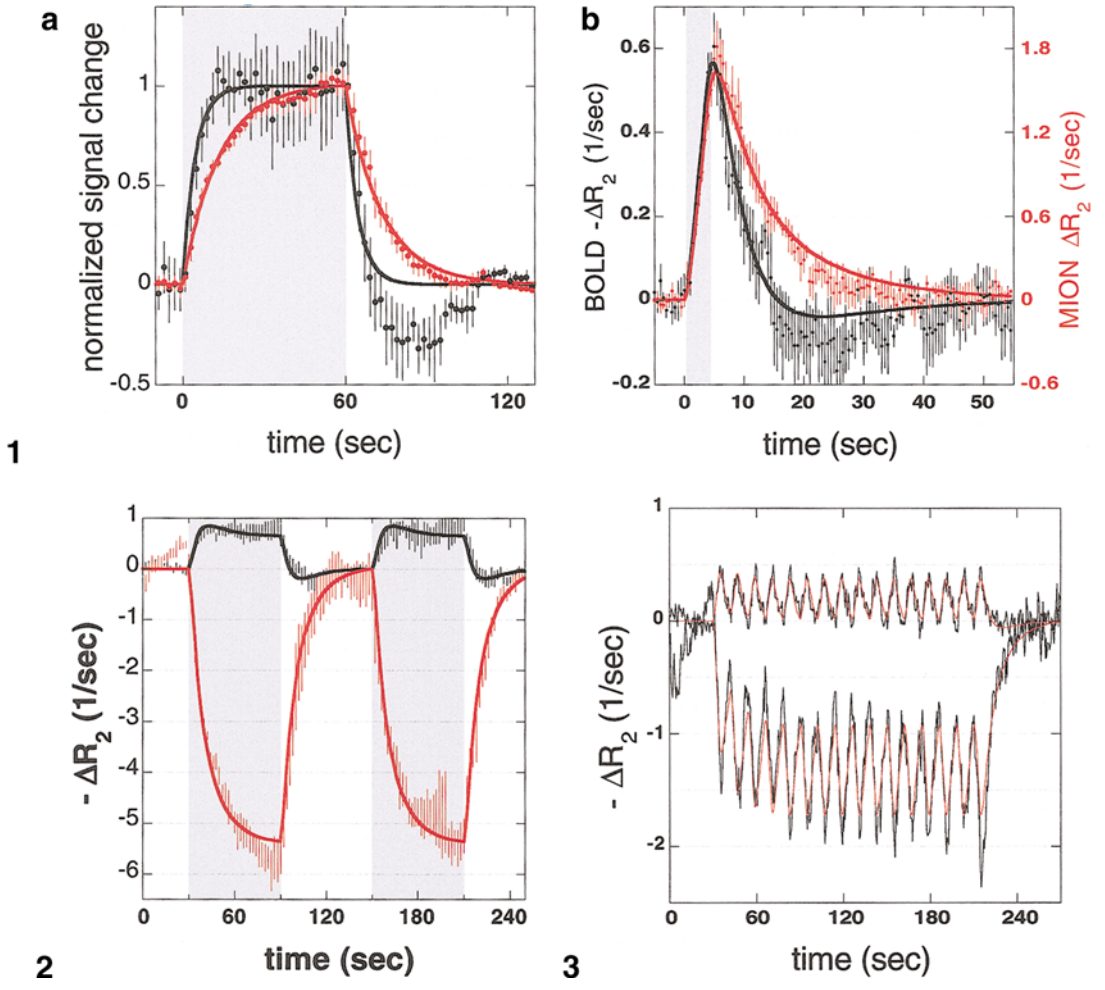

FIG. 1. (a) Normalized BOLD (black) and MION (red, reversed sign) signal changes as a function of time due to 60 s of visual stimulation (gray shaded interval). The lines are monexponential fits to the data using time constants of 4.5 s (BOLD) and 13.5 s (MION). (b) Measured impulse response functions for BOLD (black) and MION (red, reversed sign) signal using a 4-s stimulus (gray shaded interval). Solid lines indicate the linear model estimation of the response obtained by simultaneously fitting all stimulation paradigms, using the dominant time constants determined from prolonged stimulation (a).

FIG. 2. Relaxation rate changes for BOLD (black) and MION (red) contrast, together with the corresponding linear model fits, during two cycles of the 60 s of stimulus (gray shaded intervals) followed by 60 s of baseline. At the end of the stimulus interval, MION relaxation rate changes were more than 7 times greater than BOLD changes. Peak MION signal change corresponds to a 25% increase in cerebral blood plasma volume.

FIG. 3. Relaxation rate changes measured for BOLD (above *y* origin) and MION (below *y* origin) contrast during 16 cycles of 4 s of stimulus followed by 8 s of baseline. Black traces indicate data, and red traces show the linear model fit to the data. Whereas BOLD signal recovers to the baseline following each cycle, the slower MION response does not recover. In this rapidly presented stimulus paradigm, MION relaxation rate changes are slightly more than twice as large as BOLD changes.

$P_1 / [\sigma^2 / N_F \, C_{1,1}]^{1/2}$. In this equation, $\mathbf{C}$ is the covariance matrix, $\mathbf{C} = (\mathbf{B}^T\mathbf{B})^{-1}$, N_F is the number of degrees of freedom ($N - n$), and the stimulus reference vector is the first basis function corresponding to parameter P_1. The variance is calculated between the data and the fit as $\sigma^2 = \sum_t (d_t - \sum_j \boldsymbol{B}_{tj} \, \boldsymbol{P}_j)^2$, including basis functions describing the stimulus response, mean value of signal, and signal drift (slope).

Because the number of runs for each stimulus paradigm and MRI contrast type varied across sessions, we compared statistical scores by creating maps of the average values and standard errors of T scores across all runs and all sessions in each animal.

RESULTS

Transverse Relaxation Rates and MION Blood Half-Life

Within large brain volumes in monkeys M-A and M-B that were selected to avoid susceptibility artifacts, the average R_2^* value (mean ± SEM) prior to injection

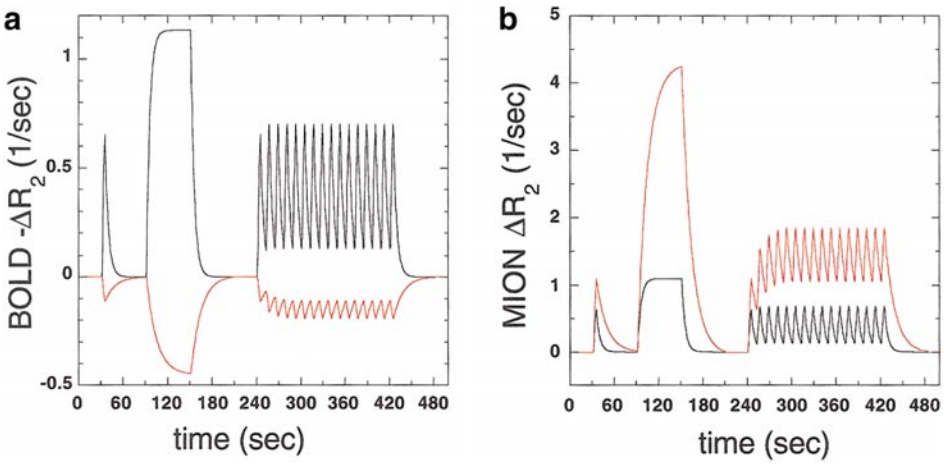

FIG. 4. A general linear model fit separated data obtained using BOLD (left) and MION (right) into a fast time response (black, 4.5 s time constant) and a slow response (red, 13.5-s time constant). Fits to the data are shown for stimuli of 4 s (first response), 60 s (second response), and a train of rapidly presented responses (4 s on, 8 s off). The total response (not shown) is the sum of the fast and slow components.

of MION was 20.9 ± 0.2 s^{-1} (T_2^* = 48 ms). However, numerous regions around the edge of the brain exhibited T_2^* values less than 20 ms. An echo time of 30 ms was selected for BOLD experiments as a compromise between functional sensitivity and susceptibility artifacts across the brain. Because adequate sensitivity can be obtained at any echo time by adjusting the dose of iron oxide agent, MION experiments employed the minimum obtainable echo time of 20 ms for our EPI sequence and resolution.

Using the average value of the relaxation rate in BOLD experiments as a reference value for zero dose of contrast agent, the mean change in relaxation rate due to the presence of MION was 24.1 ± 0.6 s^{-1} across the brain at the beginning of these experiments. During experiments lasting 2.9 ± 0.3 h, the average value of the MION-induced relaxation rate was 21.1 ± 1.1 s^{-1}, and the calculated MION blood half life was 8.4 ± 1.4 h.

Response Scores

Monkeys attended to the fixation cue and responded when the cue switched to a horizontal position. Monkey M-A correctly responded to 92 ± 10% (mean ± standard deviation) of the cues during BOLD experiments, and 85 ± 5% of the cues during MION experiments. Monkey M-B correctly responded to 89 ± 13% and 92 ± 5% of the cues during BOLD and MION experiments, respectively. The average duration of all BOLD sessions was 2.2 ± 0.4 h, and the average duration of MION sessions was 2.9 ± 0.7 h. Neither session duration nor response scores were significantly different ($P > 0.05$) between BOLD and MION sessions.

Temporal Response

Figure 1a shows the shapes of the BOLD and MION responses due to a sustained stimulus after averaging across both animals and all magnet sessions. Error bars in all figures represent standard errors of the mean across scanning sessions. The curves in the figure are single exponential fits to the data using one time constant for both the rise and decay of signal. A single exponential time constant of 13.5 s provided a good description of the low frequency MION response. A time constant of 4.5 s adequately described the low frequency BOLD response, except for the poststimulus region, which showed an undershoot with a time constant similar to the MION response. In order to better describe the post-stimulus undershoot, the exponential basis for the BOLD IRF included both the 4.5- and 13.5-s time constants. Because the single MION time constant did not provide a good description of briefly presented stimuli, and because changes in blood volume can be expected to contain an arterial time constant that is similar to the measured BOLD value, both the 4.5- and 13.5-s time constants were also included in the exponential basis for the MION IRF.

When only 2 time constants were used to fit each IRF, a delay was required between the onset of a stimulus and the onset of the hemodynamic response in order to describe the rapidly sampled data with TR = 500 ms. In the exponential basis [4.5, 13.5] using a 1.5-s delay, the best-fit IRF for the BOLD and MION data were [1.67, −0.67] and [0.20, 0.80]. These parameters represent the asymptotic contributions from two processes with different kinetics (see Methods). The delay between the stimulus design and the IRF convolution can be removed by incorporating a third time constant (the delay of 1.5 s) into the exponential basis for the IRF. The inclusion of a third exponential improved the description of the response onset immediately after stimulation. In the exponential basis described by time constants [1.5, 4.5, 13.5], the optimal BOLD IRF was found to be [−0.89, 3.09, −1.20], and

the best fit for the MION IRF was [−0.21, 0.41, 0.80]. This basis was used for fits in Figs. 1–3 and for all statistical analyses.

The average BOLD and MION responses for the 4-s stimuli, together with the respective IRF fits, are shown in Fig. 1b. Figure 2 shows data and fits for the long block stimuli of 60-s duration. In each case, a poststimulus undershoot was associated with a slow poststimulus decrease of blood volume. The enhancement in signal change was found to be a strong function of stimulus duration. For the 4-s stimuli, the peak change in MION relaxation rate exceeded the BOLD change by a factor of 3 (Fig. 1b), but the enhancement increased to a factor of 7 for a stimulus of 60-s duration (Fig. 2). Using the average value of the transverse relaxation due to MION to normalize the signal changes in this region of interest ($R_2^{*,\mathrm{MION}} = 22.3\ \mathrm{s}^{-1}$), peak changes in cerebral blood volume averaged 8% for the 4-s stimuli (Fig. 1b) and 25% for the 60 s stimuli (Fig. 2).

In a time-invariant linear system, the slower MION response should be manifest as a low-pass filter on higher stimulation frequencies. Figure 3 shows responses to repeated presentations of 4 s of stimulus followed by 8 s of baseline. This interstimulus interval is just sufficient for BOLD signal to return to baseline following each stimulus, whereas blood volume remains elevated throughout the duration of the stimulus cycle. With these parameters, BOLD cyclic relaxation rate changes were about 50% as large as those for a long block stimulus, whereas the stimulus-induced fluctuations in the MION relaxation rate were only 20% as large as those for the longer stimulus of Fig. 2.

Insight into the underlying physiology of each method can be obtained from the 2-exponential decomposition of the impulse response function. For BOLD signal, the two time constants are most simply identified as the responses of blood oxygenation and blood volume. For the MION method, the time constants presumably are related to arterial and venous dilations. The exponential decomposition of the MION signal found that the slow time constant contained 80% of the strength during prolonged stimulation. The exponential decomposition of the BOLD signal suggests that changes in CBV reduce the BOLD effect by 40% during prolonged stimulation.

Figure 4 shows the fast and slow components of the BOLD and CBV responses for each stimulus type, using a single scaling factor as determined by simultaneously fitting all the data (note that Figs. 1–3 use a separate scaling for each run, following the usual analysis procedure). By comparison of Fig. 4 with the data in Figs. 1–3, a single scaling factor well describes the BOLD data for each stimulus paradigm. The MION data is well described for the short and long stimuli, but the response to the rapidly presented stimuli is overestimated somewhat by the linear model analysis. CBV-weighted signal suffers a larger reduction in relative sensitivity than BOLD signal for short stimuli or event-related designs as compared to block stimuli, due to the slower response of CBV. Because the slow CBV response produces a negative BOLD offset that compensates the positive offset for rapidly presented stimuli, the dramatic baseline shift seen for the MION response in Fig. 3 is not evident in the BOLD data or the fitted response.

Functional Sensitivity and Spatial Localization

The use of exogenous contrast agent provided a large improvement in functional sensitivity, which depended upon both the stimulus paradigm and the spatial location within visual cortex. Figure 5 shows the average BOLD and MION functional maps in monkey M-A for a single 4.5-min run using the 60-s stimulus paradigm. The maps are based upon the average T scores across runs and scan sessions, and P values were corrected for multiple comparisons. The underlying grayscale images are the spatially smoothed echo planar images from which the functional maps were derived. The general pattern of brain activation is similar for the two methods, but the overall sensitivity of the MION method is much higher.

Figure 6 reveals several apparent differences in the functional maps for the two methods. The first panel shows statistical scores accumulated across 8 runs for 4 slices from the best BOLD functional data set in either animal. Strong BOLD signal changes occurred in the straight sinus at each level, with generally smaller significance levels for the sagital sinus. These vessel artifacts were absent in the MION maps, since this dose of contrast agent eliminates intravascular signal changes that are associated with changes in blood oxygenation. However, the BOLD maps also show activation in tissue regions, identified as areas with good signal in the MION images. These areas (e.g., last slice in Fig. 6) form a bridge between the sinuses and areas identified as activated using the MION method. Presumably, this indicates a loss of BOLD functional resolution due to venous drainage from activated tissue.

Figure 6b is a map of the ratio of MION CNR to BOLD CNR values for the last 3 slices in Fig. 5. These slices represent the most posterior aspect of primary visual cortex, where the calcarine fissue is prominent. Within a 6-mm strip centered on the calcarine fissue, BOLD significance levels were actually higher than those for the MION method, presumably as a result of the high blood volume fraction in this area near the sagital sinus.

In order to assess the degree of similarity in brain activation as assessed by the BOLD and MION methods, and to compare the functional sensitivities of the

two methods, Fig. 7 provides scatter plots of relaxation rate changes and contrast-to-noise ratios. Changes in BOLD and MION relaxation rates are compared throughout visual cortex for both animals for all voxels that show significant signal changes across runs with either method (Fig. 7a) and both methods (Fig. 7b). Signal changes in large vessels appear along the line $\Delta R_2^{*\mathrm{MION}} = 0$ in Fig. 7a. In those voxels that are activated by both methods, the dominant correlation is a linear coupling of relaxation rate changes along a line that is approximately $\Delta R_2^{*\mathrm{MION}} = 6\ \Delta R_2^{*\mathrm{BOLD}}$ using this dose of contrast agent.

Figure 7c compares the functional sensitivity of the two methods for all voxels in Fig. 7b. Low values of BOLD CNR can result from small changes in local neuronal activity or from low values of the resting blood volume fraction. The latter case accounts for voxels that exhibited a CNR enhancement greater than half an order of magnitude using exogenous agent, since the MION method has little CNR dependence on the resting state blood volume fraction (Mandeville and Marota, 1999). The highest values of BOLD CNR were predominantly associated with large resting blood volume fractions, and stimulus-induced BOLD signal changes in such areas were comparable to those obtained using the MION method.

This figure demonstrates a very practical advantage of exogenous agent at 3 Tesla in awake primates. Most voxels that were identified as activated using BOLD signal were also selected by the MION method with equal or better statistical power, whereas voxels that had low BOLD CNR values were generally those that exhibited the greatest relative signal increases due to the use of iron oxide. Figure 7d shows the one-dimensional distribution of CNR ratio averaged across animals and magnet sessions. The average increase in functional sensitivity in monkeys M-A and M-B was 3.0 and 3.3, respectively, using stimuli of 60-s duration.

For shorter stimuli or more rapid presentation rates, the increase in functional sensitivity was smaller. When short stimuli (4 s) were presented with a long inter-stimulus interval (26 s), the average sensitivity of the MION method was only 1.7 times greater than that of the BOLD method (M-A: 1.5, M-B: 1.9). Figure 3 demonstrates that short, rapidly presented stimuli may experience even greater reduction of MION sensitivity. For this particular stimulus paradigm, however, MION provided better than a factor of 2 improvement over the BOLD method, due to the inclusion of baseline samples at the beginning and end of the run.

DISCUSSION

This study investigated the viability and quantified the advantages of employing an iron oxide contrast agent with a long blood half life to enhance functional brain imaging for repeated studies in awake, behaving primates. The viability of this approach was assessed by a series of experiments in two animals using MION contrast agent. The sensitivity and temporal response were compared to the common BOLD technique at a field strength of 3 Tesla using a variety of stimulus timings. Whereas the MION method works well in awake primates even at 1.5 Tesla (Vanduffel *et al.*, 2001), the use of a 3 Tesla scanner in this study elevated BOLD signal to a sufficient level for quantitative spatiotemporal comparisons with the MION signal. Significantly, MION injection did not produce adverse behavioral effects, as assessed by response scores and session duration, and no obvious long term health problems have been encountered. In accordance with results obtained in anesthetized rodent models, the use of iron oxide greatly improved the quality and consistency of functional brain maps by increasing the magnitude of signal changes.

Temporal Response

This study employed a short stimulus to determine the impulse response function, a long stimulus to evaluate the asymptotic response, and a rapidly modulated stimulus to simulate an event-related design. Results showed that BOLD and CBV temporal responses differed significantly in the awake macaque, supporting the view arising from MRI studies in anesthetized rodents (Mandeville *et al.*, 1999b, 1999a).

By decomposing the BOLD kinetics into two dominant processes, it was estimated that CBV changes reduce BOLD signal by about 40% during prolonged stimulation, in agreement with other empirical estimates based upon the use of exogenous contrast agent (35% (Kennan *et al.*, 1998)), (36% (Mandeville *et al.*, 1999a)), (46% (Scheffler *et al.*, 1999)). Due to intravascular contributions to BOLD signal (T_2^* changes in the blood), this estimate is expected to be somewhat dependent upon the magnetic field strength. By decomposing the MION kinetics into two dominant processes, 80% of the strength during prolonged stimulation was attributed to a process that evolved more slowly than BOLD signal, and thus more slowly than blood flow and arterial dilation. However, if the rapid component of CBV change also contains a contribution from the elastic dilation of capillaries and veins (Mandeville *et al.*, 1999b), then arterial dilation contributes less than 20% of total blood volume changes during prolonged stimulation.

As in the anesthetized rodent, the temporal characteristics of the signal implicate venous blood volume as a source of the BOLD poststimulus undershoot, which may also have a neuronal contribution that modulates blood flow (Hoge *et al.*, 1999). Of course, the underlying

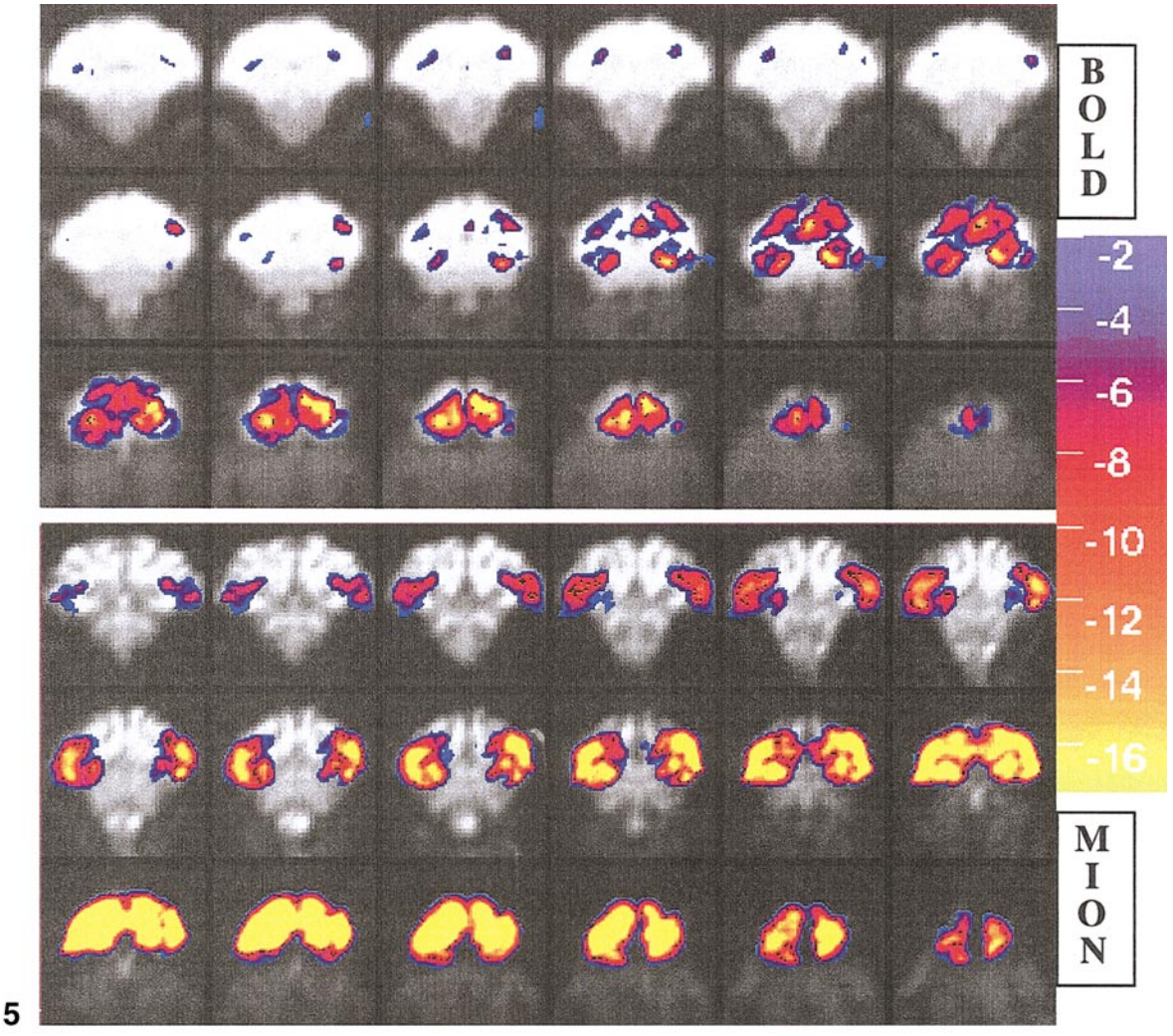

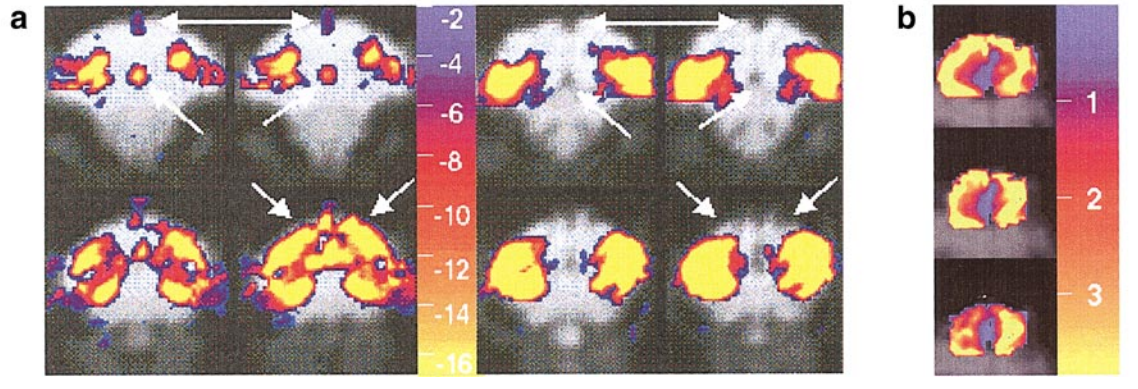

FIG. 5. Representative (average) functional brain maps obtained in an awake, behaving primate (M-A) during single 4.5-min runs using either BOLD (top) or MION (bottom) contrast. The color scale shows the log of p values from a *T* test after correcting for multiple comparisons, and the grayscale shows echo planar images from each data set. The stimulus consisted of 2 cycles of 60 s of a flashing checkerboard followed by 60 s of baseline.

FIG. 6. (a) Slices 3,4,9, and 10 from Figure 5 after averaging across runs. BOLD functional maps (left, 8 runs) show contributions from the straight sinus and the superior sagital sinus, which are not in evidence in the MION functional maps (right, 3 runs). Moreover, BOLD signal changes appear in tissue that bridges the venous sinuses and areas identified as activated by the MION technique. (b) The ratio of MION CNR to BOLD CNR is shown as color overlay on the last three slices in Fig. 5. BOLD sensitivity exceeds that for the MION method within a 6-mm strip centered on the calcarine fissue, presumably due to the high blood volume fraction in this area near the sagital sinus.

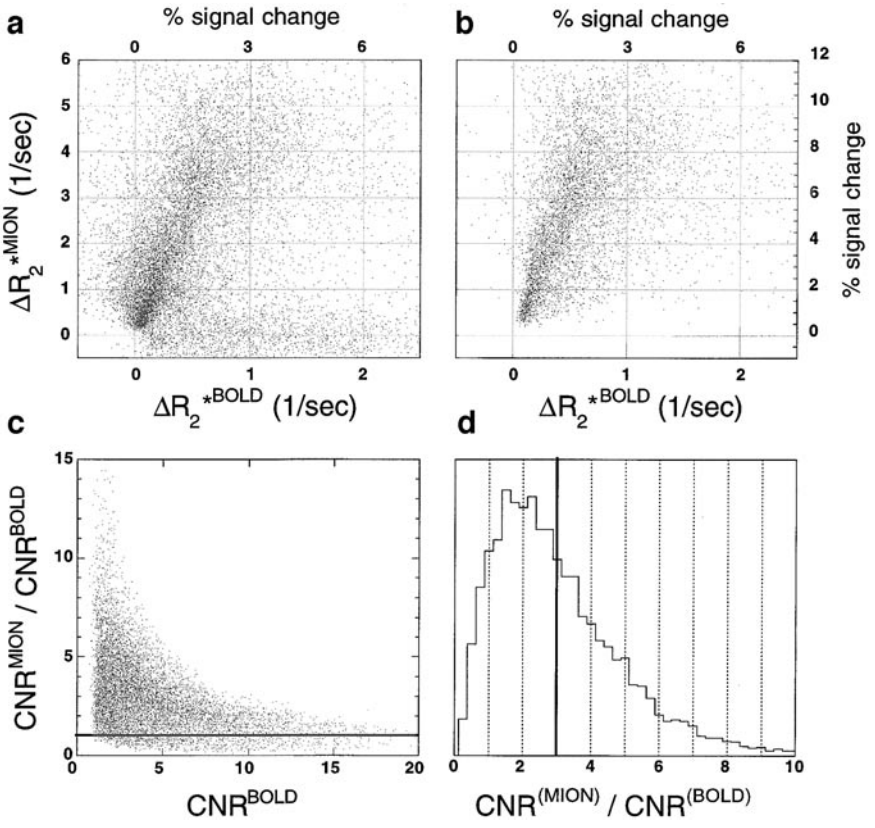

FIG. 7. (a) A scatter plot of all voxels in primate brain that were activated by either the BOLD or the MION methods after registering across sessions and averaging across monkeys. (b) Those voxels that were activated by both methods. Changes in relaxation rates were related in an approximately linear way for most voxels, but a significant fraction did not adhere to this relationship. (c) The sensitivity enhancement for all voxels in panel "b" as a function of the BOLD contrast-to-noise ratio. (d) A histogram of the ratio of functional sensitivities of the two methods. The MION method increased the functional contrast-to-noise ratio by a mean factor of 3, and a most likely factor of 2.

temporal dynamics of neuronal activity can be expected to influence the temporal response of CBV as well as BOLD signal. However, the general shape of the CBV response was quite consistent across brain structures in this study, and a very similar response was obtained by Vanduffel *et al.* (2001) despite the use of different stimuli.

Whatever the exact mechanism of the temporal smoothing applied to the response of cerebral blood plasma volume, this study demonstrates that CBV-weighted fMRI is amenable to a general linear model analysis. The slow response of CBV relative to BOLD signal implies that CBV is particularly advantageous for long stimuli in terms of detection sensitivity, since short or rapidly presented stimuli may not reach a maximum response.

Functional Sensitivity and Spatial Localization

Previous studies in anesthetized rodents using iron oxide contrast agents have demonstrated a large increase in functional sensitivity relative to BOLD signal (Mandeville *et al.,* 1998; Kennan *et al.,* 1998). The sensitivity enhancement is a strong function of the local blood volume fraction due to the different "vascular filters" of the BOLD and MION methods (Mandeville and Marota, 1999; Mandeville *et al.,* 2001a). This study confirmed these results in the absence of anesthesia in a primate species. The use of MION contrast agent increased functional sensitivity relative to BOLD signal at 3 Tesla by a mean factor of 3 across macaque visual cortex for a long stimulus. The dose of contrast agent, local blood volume fraction, magnetic field strength, resting state blood oxygenation, and duration and separation of stimuli are among the factors which influence the degree by which exogenous contrast agent boosts the size of absolute signal changes relative to the BOLD method.

The dose of contrast agent alters the transverse relaxation rate of MRI signal as $R_2^{*,\mathrm{TOTAL}} = R_2^{*,\mathrm{endogenous}} + R_2^{*,\mathrm{MION}}$, where $R_2^{*,\mathrm{MION}}$ depends upon dose in a nearly linear way (Kennan *et al.,* 1994; Boxerman *et al.,* 1995). The sensitivity for functional imaging should depend roughly upon the function $T_E R_2^{*,\mathrm{MION}} \exp(-T_E R_2^{*,\mathrm{MION}})$, where $R_2^{*,\mathrm{MION}}$ represents the value across a large brain

volume in order to account for regional variations in the parenchymal blood volume fraction. In this study, we chose the minimum obtainable echo time of 20 ms for our single shot EPI sequence in order to minimize susceptibility artifacts. The selected iron dose ($T_E R_2^{*,MION} \sim 0.4$) was on the low side of the sensitivity curve (theoretical maximum at $T_E R_2^{*,MION} = 1$) in order to reduce the injected iron and to maintain an acceptable signal to noise ratio, while still delivering about 70% of the CNR advantage. These results suggest that 10 mg/kg is a suitable iron dose using an echo time of about 20 ms for this agent in monkeys, results that are comparable with previous rat studies. Since the induced magnetization of MION saturates as a function of field strength (Shen *et al.*, 1993), the optimal MION dose should be roughly independent of field above 1.5 Tesla.

Resting state venous blood oxygenation is the analogue of iron dose for the BOLD method. Because all anesthetics decrease venous oxygenation (Michenfelder, 1988), which depends upon the ratio of oxygen utilization to blood flow, BOLD imaging can be expected to have a slightly higher sensitivity in the awake state than in the presence of anesthesia for the same fractional change in blood flow. The anesthesia-induced reduction of BOLD sensitivity should be most pronounced for the inhalational vasodilators like halothane, isoflourane, and desflourane, which decrease metabolic rate but increase cerebral blood flow above the nonanesthetized state. This suggests that the advantages of the MION method should be somewhat greater in the anesthetized state relative to awake studies. Nevertheless, the threefold increase in sensitivity provided by MION in the awake macaque at 3 Tesla is not far out of line with results from anesthetized rodents (Mandeville *et al.*, 1998, 2001a; Chen *et al.*, 2001) after scaling for differences in magnetic field strength.

Based upon these results at 3 Tesla, we expect that a similar choice of experimental parameters at 1.5 Tesla should increase sensitivity relative to the BOLD method by a factor of approximately 6. Vanduffel *et al.* (2001) found that a slightly lower MION dose boosted absolute signal changes by a factor of 5 relative to BOLD signal in motion-sensitive visual regions during prolonged stimulation. This would correspond to a fivefold increase in sensitivity, in good agreement with projections based upon our 3 Tesla data, if we assume that injection of MION leaves the noise unaltered. Dubowitz *et al.* (2001) reported a threefold increase in percentage signal changes and a twofold reduction of baseline signal, corresponding to a CNR increase of about 1.5. This lower value is presumably due to the short stimulus duration, lower dose of contrast agent, and longer echo time used in that study.

Although the spatial patterns of brain activation observed using the BOLD and MION methods were quite similar, differences were also apparent. Large venous sinuses showed changes in BOLD signal, whereas MION signal was extinguished in such areas by the large dose of contrast agent. While such obvious BOLD vascular artifacts usually will not be misidentified as activated tissue, some tissue regions also exhibited BOLD but not MION signal changes, a result presumably indicating downstream dilution of deoxyhemoglobin and degradation of BOLD functional resolution. It is much more difficult to assess whether local blood volume changes can occur without changes in deoxyhemoglobin at the spatial resolution used in this study, since the much higher sensitivity of the MION method reveals activation that may be below the BOLD threshold.

Finally, it's important to note that intrasubject and intersubject comparisons using repeated injections of a contrast agent like MION need to monitor the blood dose of agent during each session in order to correct for cross-session differences in the blood concentration of iron. This consideration becomes important if different doses are used, or whenever the dose of agent administered during one session does not have time to clear the bloodstream before the subsequent imaging session. Cross-session comparisons either can rely upon percent calculations in CBV or global normalization of relaxation rates, as described in the methods, with the latter being better suited for studies that cannot, for logistical reasons, obtain both pre-injection and post-injection baselines of signal within the same session. Cross-session statistical comparisons, on the other hand, can be biased by differences in iron dose in a way that cannot be corrected retrospectively. To prevent systematic differences in statistical power from biasing group average results, blood iron concentrations should be as consistent as possible across sessions, and ideally one should use doses near the optimal dose (iron-induced signal attenuation of e^{-1}), since that choice minimizes the dependence of statistical power on iron dose.

Iron Accumulation and Management

In human studies, dextran-coated ultrasmall superparamagnetic iron oxides (USPIOs) similar to MION have shown very low toxicity at doses up to 4 mg-Fe/kg (Taylor *et al.*, 1999). Agents currently in clinical trials include AMI-227 (Advanced Magnetics Inc., Cambridge, MA) for imaging liver or splenic lesions (Sharma *et al.*, 1999) and NC100150 (Nycomed Imaging, Oslo, Norway) for coronary angiography (Taylor *et al.*, 1999).

In repeated primate experiments using high iron doses for brain imaging as reported here, the primary concerns are (1) the development of an immune response to dextran, and (2) the gradual accumulation of iron in excess of body requirements. There was no

evidence of allergic reaction during these studies, and the total injected iron dose during these series is considered insufficient to cause acute or long term adverse effects. In humans, the normal level of total body iron is roughly 60 mg/kg, the maximum natural rate of iron excretion in a nonmenstruating adult is about 10 mg/kg/year, and the liver is the repository for 90% of excess iron (Leggett *et al.*, 2000; Barton *et al.*, 2000). Thus, we estimate that total iron doses of 40–60 mg/kg in the two animals increased body iron stores by a factor of about 2. While iron metabolism is imperfectly understood, the results of chronic iron overload have been studied for decades due to genetic diseases that elevate liver and total body iron stores by an order of magnitude relative to normal levels for many years (Edwards *et al.*, 2000; Olivieri and Brittenham, 1997).

For continued studies that deposit much more contrast agent, iron monitoring and management should form an important part of the protocol. Monitoring can be achieved by sampling blood transferrin saturation and total blood iron concentration (Olivieri and Brittenham, 1997). MRI provides the highest sensitivity for noninvasive assessment of liver iron, with a detection threshold of 2 to 3 times normal liver iron levels (Guyader and Gandon, 2000; Bonkovsky *et al.*, 1999). Phlebotomy, the standard treatment for hemochromatosis, removes about 4 mg/kg iron per week by withdrawing about 7 ml blood per kg (Barton *et al.*, 2000). Additional iron can be removed by desferoxamine chelation, which preferentially targets stored iron in liver parenchyma and other tissues, with no effect on hemoglobin iron and little affinity for transferrin-bound iron (Herschko *et al.*, 2000). This method can be used to minimize or reverse iron overload without worry of causing iron deficiency. However, long term use of very high doses of desferoxamine can produce adverse effects and should be avoided (Herschko *et al.*, 2000; Olivieri and Brittenham, 1997). For the treatment of the genetic disorder thalassemia major, a suggested goal for desferoxamine chelation therapy is maintenance of total body iron stores within a factor of about 5 times normal levels (Olivieri and Brittenham, 1997).

The experience from the human population suggests that repeated fMRI studies using iron oxide contrast agent can be performed in this primate model until total body stores increase by several factors without worry of significant health complications. However, subcutaneous injections of an iron chelator should be considered as a method to prevent iron stores from reaching unacceptable levels. Vanduffel *et al.* have now injected as much as 166 mg/kg iron into a single monkey (personal communication) and measured normal blood iron levels after desferoxamine treatment ("desferal," Novartis Pharma AG, Basle, Switzerland). No significant adverse behavioral effects have been observed in those monkeys after more than 1 year from the first MION injection.

Conclusions

Our results demonstrate that functional MRI can be performed reliably on awake, behaving macaques at a field strength of 3 Tesla using a commercial horizontal bore MRI system. Although BOLD activation maps of reasonable quality were obtained with sufficient averaging, the use of MION contrast agent significantly increased stimulus-correlated signal changes, thereby improving the quality and reliability of results. We did not observe any obvious adverse effects on the monkeys' health due to MION injection. However, we expect that iron monitoring and management will be necessary for a long-term program of repeated fMRI studies using iron oxide in these animals.

ACKNOWLEDGMENTS

The authors gratefully acknowledge financial support from the National Foundation for Functional Brain Imaging (U.S.A.), from the National Institutes of Health (J.B.M.: R01-RR14543A02; A.M.D.: R01-RR13609, P41-RR14075, R01-NS39581), from the Queen Elisabeth Medical Foundation (GSKE), and from the Flemish Regional Ministry of Education (G.A.O.: GOA 2000/11).

REFERENCES

Barton, J. C., McDonnell, S. M., Adams, P. C., Brissot, P., Powell, L. W., Edwards, C. Q., Cook, J. D., and Kowdley, K. V. 2000. Management of hemochromatosis. In *Hemochromatosis: Genetics, Pathophysiology, Diagnosis, and Treatment* (J. C. Barton and C. Q. Edwards, Ed(s.), pp. 329–338. Cambridge Univ. Press, Cambridge, UK.

Bonkovsky, H. L., Rubin, R. B., Cable, E. E., Davidoff, A., Pels Rijcken, T. H., and Stark, D. D. 1999. Hepatic iron concentration: Nonivasive estimation by means of MR Imaging techniques. *Radiology* **212:** 227–234.

Boxerman, J. L., Hamberg, L. M., Rosen, B. R., and Weisskoff, R. M. 1995. MR contrast due to intravascular magnetic susceptibility perturbations. *Magn. Reson. Med.* **34:** 555–566.

Boynton, G. M., Engel, S. A., Glover, G. H., and Heeger, D. J. 1996. Linear systems analysis of functional magnetic resonance imaging in human V1. *J. Neurosci.* **16:** 4207–4221.

Chen, Y. I., Mandeville, J. B., Nguyen, T. V., Talele, A., Cavagna, F., and Jenkins, B. G. 2001. Improved mapping of pharmacologically induced neuronal activation using the IRON technique with superparamagnetic iron blood pool agents. *J. Magn. Reson. Imag.* **14:** 517–524.

Cox, R. W., and Hyde, J. S. 1997. Software tools for analysis and visualization of FMRI data. *NMR Biomed.* **10:** 171–178.

Disbrow, E. A., Slutsky, D. A., Roberts, T. P., and Krubitzer, L. A. 2000. Functional MRI at 1.5 tesla: a comparison of the blood oxygenation level-dependent signal and electrophysiology. *Proc. Natl. Acad. Sci. USA* **97:** 9718–9723.

Dubowitz, D. J., Bernheim, K. A., Chen, D.-Y., Bradley, Jr., W. G., and Andersen, R. A. 2001. Enhancing fMRI contrast in awake-behaving primates using intravascular magnetite dextran nanoparticles. *NeuroReport* **12:** 2335–2340.

Dubowitz, D. J., Chen, D. Y., Atkinson, D. J., Grieve, K. L., Gillikin, B., Bradley, W. G. J., and Andersen, R. A. 1998. Functional magnetic resonance imaging in macaque cortex. *Neuroreport* **9:** 2213–2218.

Edwards, C. Q., Griffen, L. M., Bulaj, Z. J., Ajioka, R. S., and Kushner, J. P. 2000. Estimate of the frequency of morbid complications of hemochromatosis. In *Hemochromatosis: Genetics, Pathophysiology, Diagnosis, and Treatment* (J. C. Barton, and C. Q. Edwards, Eds.), pp. 312–317. Cambridge Univ. Press, Cambridge, U.K.

Enochs, W. S., Harsh, G., Hochberg, F., and Weissleder, R. 1999. Improved delineation of human brain tumors on MR images using a long-circulating, superparamagnetic iron oxide agent. *J. Magn. Reson. Imag.* **9:** 228–232.

Friston, K. J., Holmes, A. P., Worsley, K. J., Poline, J. P., Frith, C. D., and Frackowiak, R. S. J. 1995. Statistical parametric maps in functional imaging: A general linear approach. *Hum. Brain Mapp.* **2:** 189–210.

Guyader, D., and Gandon, Y. 2000. Computed tomography and magnetic resonance imaging in the diagnosis of hemochromatosis. In *Hemochromatosis: Genetics, Pathophysiology, Diagnosis, and Treatment* (J. C. Barton, and C. Q. Edwards, Ed(s), pp. 219–225. Cambridge Univ. Press, Cambridge, UK.

Hayashi, T., Konishi, S., Hasegawa, I., and Miyashita, Y. 1999. Short communication: mapping of somatosensory cortices with functional magnetic resonance imaging in anaesthetized macaque monkeys. *Eur. J. Neurosci.* **11:** 4451–4456.

Herschko, C., Link, G., and Konijn, A. M. 2000. Chelation therapy in iron overload. In *Hemochromatosis: Genetics, Pathophysiology, Diagnosis, and Treatment* (J. C. Barton, and C. Q. Edwards, Eds.), pp. 339–354. Cambridge Univ. Press, Cambridge, UK.

Hoge, R. D., Atkinson, J., Gill, B., Crelier, G. R., Marrett, S., and Pike, G. B. 1999. Stimulus-dependent BOLD and perfusion dynamics in human VI. *NeuroImage* **9:** 573–585.

Josephson, L., Groman, E. V., Menz, E., Luis, J. M., and Bengele, H. 1990. A functionalized superparamagnetic iron oxide colloid as a receptor directed MR contrast agent. *Magn. Reson. Imag.* **8:** 637.

Kennan, R. P., Scanley, B. E., Innis, R. B., and Gore, J. C. 1998. Physiological basis for BOLD MR signal changes due to neuronal stimulation: Separation of blood volume and magnetic susceptibility effects. *Magn. Reson. Med.* **40:** 840–846.

Kennan, R. P., Zhong, J., and Gore, J. C. 1994. Intravascular Susceptibility Contrast Mechanisms in Tissues. *Magn. Reson. Med.* **31:** 9–21.

Leggett, R. W., Barton, J. C., and Eckerman, K. F. 2000. Mathematical models of metal metabolism in hemochromatosis. In *Hemochromatosis: Genetics, Pathophysiology, Diagnosis, and Treatment.* (J. C. Barton, and C. Q. Edwards, Eds.), pp. 170–176. Cambridge Univ. Press, Cambridge, UK.

Logothetis, N. K., Guggenberger, H., Peled, S., and Pauls, J. 1999. Functional imaging of the monkey brain. *Nat. Neurosci.* **2:** 555–562.

Logothetis, N. K., Pauls, J., Augath, M., Trinath, T., and Oeltermann, A. 2001. Neurophysiological investigation of the basis of the fMRI signal. *Nature* **12:** 150–157.

Mandeville, J. B., Jenkins, B. G., Kosofsky, B. E., Moskowitz, M. A., Rosen, B. R., and Marota, J. J. A. 2001a. Regional sensitivity and coupling of BOLD and CBV changes during stimulation of rat brain. *Magn. Reson. Med.* **45:** 443–447.

Mandeville, J. B., and Marota, J. J. A. 1999. Vascular filters of functional MRI: Spatial localization using BOLD and CBV contrast. *Magn. Reson. Med.* **42:** 591–598.

Mandeville, J. B., Marota, J. J. A., Ayata, C., Moskowitz, M. A., Weisskoff, R. M., and Rosen, B. R. 1999a. An MRI measurement of the temporal evolution of relative CMRO2 during rat forepaw stimulation. *Magn. Reson. Med.* **42:** 944–951.

Mandeville, J. B., Marota, J. J. A., Ayata, C., Zaharchuk, G., Moskowitz, M. A., Rosen, B. R., and Weisskoff, R. M. 1999b. Evidence of a cerebrovascular post-arteriole windkessel with delayed compliance. *J. Cereb. Blood Flow Metab.* **19:** 679–689.

Mandeville, J. B., Marota, J. J. A., Kosofsky, B. E., Keltner, J. R., Weissleder, R., Rosen, B. R., and Weisskoff, R. M. 1998. Dynamic functional imaging of relative cerebral blood volume during rat forepaw stimulation. *Magn. Reson. Med.* **39:** 615–624.

Mandeville, J. B., Vanduffel, W., Fize, D., Nelissen, K., Rosen, B. R., Tootell, R. B., Van Hecke, P., and Orban, G. A. 2001b. Enhanced fMRI using iron oxide contrast agent in awake, behaving primates. *In Int. Soc. Magn. Reson. Med.* p. 1334. Glasgow, Scotland, UK.

Michenfelder, J. D. 1988. *Anesthesia and the Brain*. Churchill Livingstone, New York.

Olivieri, N. F., and Brittenham, G. M. 1997. Iron-chelating therapy and the treatment of thalassemia. *Blood* **89:** 739–761.

Scheffler, K., Seifritz, E., Haselhorst, R., and Bilecen, D. 1999. Titration of the BOLD effect: Separation and quantitation of blood volume and oxygenation changes in the human cerebral cortex during neuronal activation and ferumoxide infusion. *Magn. Reson. Med.* **42:** 829–36.

Sharma, R., Saini, S., Ros, P. R., Hahn, P. F., Small, W. C., de Lange, E. E., Stillman, A. E., Edelman, R. R., Runge, V. M., Outwater, E. K., Morris, M., and Lucas, M. 1999. Safety profile of ultrasmall superparamagnetic iron oxide ferumoxtran-10: Phase II clinical trial data. *J. Magn. Reson. Imag.* **9:** 291–294.

Shen, T., Weissleder, R., Papisov, M. A., Bogdanov, J., and Brady, T. J. 1993. Monocrystalline Iron Oxide Nanocompounds (MION): Physiochemical Properties. *Magn. Reson. Med.* **29:** 599–604.

Stefanacci, L., Reber, P., Costanza, J., Wong, E., Buxton, R., Zola, S., Squire, L., and Albright, T. 1998. fMRI of monkey visual cortex. *Neuron* **20:** 1051–1057.

Taylor, A. M., Panting, J. R., Keegan, J., Gatehouse, P. D., Amin, D., Jhooti, P., Yang, G. Z., McGill, S., Burman, E. D., Francis, J. M., Firmin, D. N., and Pennell, D. J. 1999. Safety and preliminary findings with the intravascular contrast agent NC100150 injection for MR coronary angiography. *J. Magn. Reson. Imag.* **9:** 220–227.

van Bruggen, N., Busch, E., Palmer, J. T., Williams, S. P., and de Crespigny, A. J. 1998. High-resolution functional magnetic resonance imaging of the rat brain: Mapping changes in cerebral blood volume using iron oxide contrast media. *J. Cereb. Blood. Flow Metab.* **18:** 1178–1183.

Vanduffel, W., Fize, D., Mandeville, J. B., Nelissen, K., Van Hecke, P., Rosen, B. R., Tootell, R. B. H., and Orban, G. A. 2001. Visual motion processing investigated using contrast-enhanced fMRI in awake behaving monkeys. *Neuron* **32:** 565–577.

Vanduffel, W. J. M., Beatse, E., Nelissen, K., Tootell, R. B. H., Todd, J. T., and Orban, G. A. 2000. Areas involved in extracting structure from motion: An fMRI study in the awake fixating monkey. In *Soc. Neurosci. Abstr.*, p. 593. New Orleans LA.

Weissleder, R., Elizondo, G., and Wittenberg, K. 1990. Ultrasmall superparamagnetic iron oxide. Characterization of a new class of contrast agents for MR imaging. *Radiology* **175:** 489–493.